Crystal Structure and Immunoglobulin G Binding Properties of the Human Major Histocompatibility Complex-Related Fc Receptor[†,‡]

Anthony P. West, Jr., and Pamela J. Bjorkman*

Division of Biology 156-29 and Howard Hughes Medical Institute, California Institute of Technology, Pasadena, California 91125

Received April 3, 2000

ABSTRACT: The neonatal Fc receptor (FcRn) performs two distinct but related functions: transport of maternal immunoglobulin G (IgG) to pre- or neonatal mammals, thus providing passive immunity, and protection of IgG from normal serum protein catabolism. FcRn is related to class I MHC proteins but lacks a functional peptide binding groove. The crystal structure of human FcRn has been determined at 2.7 Å resolution and compared to the previously described structure of rat FcRn [Burmeister et al. (1994) *Nature 372*, 336–343] and to the structures of MHC and MHC-related proteins. Human FcRn is structurally similar to the rat receptor but does not form receptor dimers in the crystals as observed in crystals of rat FcRn. The interaction between human FcRn and IgG was characterized by determining the binding stoichiometry using equilibrium gel filtration and by deriving binding affinities for the different human IgG subclasses using a surface plasmon resonance assay. Like rat and mouse FcRn, human FcRn interacts with IgG with a 2:1 receptor:ligand stoichiometry. The binding of human FcRn to the four human IgG subclasses shows subclass and allotype variations but no clear subclass affinity differences that correlate with serum half-lives. The structure of human FcRn and studies of its ligand binding are relevant to current efforts to use FcRn-mediated regulation of IgG half-life in serum to increase the lifetimes of antibody-based therapeutics.

The neonatal Fc receptor (FcRn)[1] provides the fetus or newborn with passive immunity to antigens encountered by the mother by supplying the offspring with maternal antibodies, specifically immunoglobulin G (IgG) (reviewed in refs *1–3*). In rodents, transfer of immunity occurs primarily after birth, through FcRn-mediated transport of maternal IgG in ingested milk across the small intestine of the neonate. Humans acquire maternal IgG before birth by transport across the placenta, which is thought to be mediated by placental FcRn (*4*). In addition to its role in transfer of maternal IgG to pre- and neonatal animals, recent results suggest that FcRn functions throughout life as the receptor responsible for protecting circulating IgG from degradation (*5–7*). FcRn has been characterized in the rat (*8, 9*), mouse (*10*), human (*4*), and cow (*11*). All forms of FcRn show pH-dependent binding to the Fc portion of IgG, such that binding is observed at acidic (pH = 6.5), but not basic, pH. The pH dependence of the FcRn interaction with IgG ensures that FcRn binds to IgG in intracellular acidic compartments but releases IgG rapidly upon encountering the slightly basic pH (~7.4) of the extracellular milieu. In cases in which FcRn functions in the absence of an external pH gradient, such as placental transport or as a protection receptor, IgG enters acidified endosomes following fluid-phase endocytosis, binds to FcRn, and is transported to the cell surface where it dissociates to enter the bloodstream. Thus, pH-dependent binding is critical for all functions of FcRn.

FcRn is a heterodimer composed of two polypeptide chains: a transmembrane chain related to the heavy chains of class I major histocompatibility complex (MHC) molecules and the light chain β2-microglobulin (β2m) (*8, 9*), which also serves as a subunit of class I MHC proteins. Previous structural studies focused upon the rat form of FcRn (rFcRn). The 2.2 Å crystal structure of rFcRn (*12*) confirmed an MHC class I-like fold with the notable exception that rFcRn contains a narrowed and nonfunctional version of the MHC peptide binding groove (*12*). An unexpected feature of the crystal structures of rFcRn alone (*12*) and a low-resolution structure of the complex between rFcRn and Fc (*13*) was the presence of receptor dimers, which were suggested to be important for FcRn function (*14*). The rFcRn dimer interface is mediated by several intermolecular electrostatic interactions and an ordered carbohydrate from an N-linked glycoside at the dimer interface (*15*) (Figures 1 and 3A). The extracellular region of human FcRn (hFcRn) shares 68% amino acid sequence identity with rFcRn (*4*), but many of the residues involved in the rFcRn dimer interface are not conserved in the hFcRn sequence, and hFcRn lacks the N-linked carbohydrate attachment site implicated in rFcRn dimerization. To further explore the structural requirements for FcRn function and dimerization, we expressed a soluble

[1] Abbreviations: β2m, β2-microglobulin; bFcRn, bovine FcRn; CHO, Chinese hamster ovary; Fc, Fc fragment from immunoglobulin G; FcRn, Fc receptor, neonatal; hFcRn, human FcRn; IgG, immunoglobulin G; K_D, equilibrium dissociation constant; rFcRn, rat FcRn; RU, resonance units.
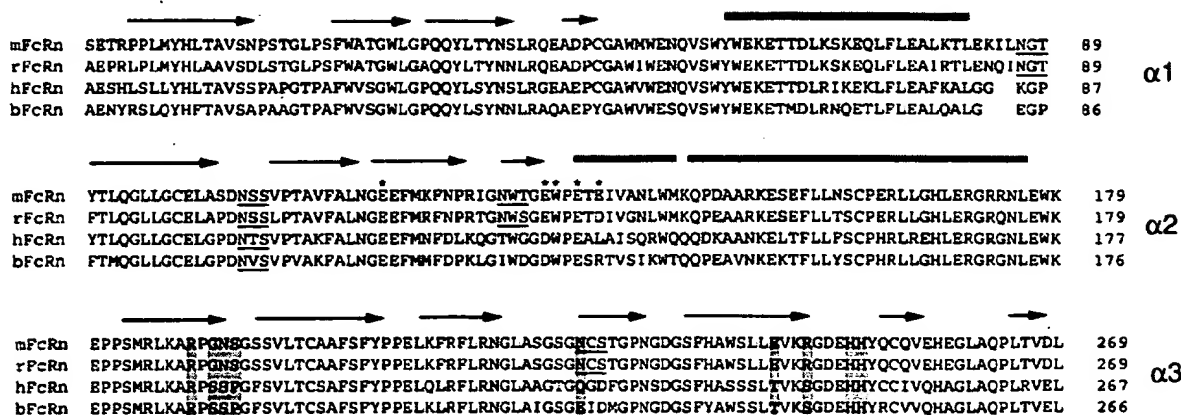
FIGURE 1: Alignment of the human (*4*), rat (*9*), mouse (*10*), and bovine (*11*) FcRn sequences. Potential N-linked glycosylation sites are underlined. Residues at the interface between rFcRn and Fc, as determined by site-directed mutagenesis (*42*) and the low-resolution rFcRn−Fc cocrystal structure (*13*), are labeled with asterisks. Residues at the interface of the rFcRn dimer of heterodimers are shaded. Crystallographically determined secondary structural elements are shown above the sequences as arrows for β-strands and solid bands for α-helical regions.

version of hFcRn, determined its crystal structure, and characterized its interaction with human IgG. We find that hFcRn is structurally similar to rFcRn but does not form dimers in the crystals. As also found for soluble versions of rFcRn and mouse FcRn (mFcRn) (*16*, *17*), two molecules of hFcRn bind to each IgG, resulting in a 2:1 binding stoichiometry. The binding affinities of hFcRn for the four subclasses of human IgG were examined using a surface plasmon resonance (SPR) based assay. These results are discussed in light of the serum half-life properties of the IgG subclasses.

MATERIALS AND METHODS

Expression and Purification of hFcRn. A construct encoding a soluble portion of hFcRn (residues 1−267 of the mature protein) was made by PCR and subcloned after sequencing into the expression vector pBJ5-GS, which contains a glutamine synthetase gene as a selectable marker and means of gene amplification (*18*). This construct and a human β2m expression vector (*19*) were cotransfected into Chinese hamster ovary (CHO) cells. Selection, amplification, and maintenance of methionine sulfoximine-resistant cells expressing FcRn/β2m heterodimers were done as described previously (*20*). Media supernatants were collected from 10 cm plates every 2−3 days. hFcRn was isolated from supernatants using a functional purification scheme based upon pH-dependent binding to an IgG column, as previously employed for purification of rFcRn (*20*). In brief, supernatants were acidified to pH 5.8 and then passed over a human IgG column, prepared by coupling 100 mg of human IgG (Sigma) to a 12 mL packed volume of CNBr-activated Sepharose (Pharmacia) as per the manufacturer's instructions. After extensive washing with a pH 5.8 Bis-Tris solution, FcRn was eluted with 50 mM Tris, pH 8.1. This material was further purified using a Uno-Q1 column (Bio-Rad). The protein was bound to the column at pH 8, and a pH gradient eluted hFcRn between pH 6.5 and pH 7.0. N-Terminal sequence analysis of purified hFcRn revealed the first 11 residues of the mature forms of the hFcRn heavy chain and human β2m. Thus, human β2m does not exchange for endogenous hamster β2m or bovine β2m present in the medium. hFcRn migrates on an SDS−PAGE gel with two

bands, an upper band of apparent molecular mass 32 kDa, corresponding to the truncated heavy chain, and a lower band of apparent molecular mass 12 kDa, corresponding to β2m (data not shown). The increase in apparent molecular mass of the heavy chain compared to that predicted from the protein sequence (29.7 kDa) presumably corresponds to N-linked carbohydrate attached to Asn 102.

IgG Reagents. Human IgG derived from serum (a mixture of the four human IgG subclasses) (Sigma) was used for equilibrium gel filtration experiments. Purified human IgG subclasses were purchased from Calbiochem (IgG1, IgG2, IgG3, and IgG4) and Sigma (IgG2, IgG3, and IgG4). All of the purified subclass proteins contained the κ light chain, except for the Calbiochem IgG3, which had a λ light chain. Each of the proteins purchased from Calbiochem was obtained from a single myeloma patient and thus should consist of a single allotype. No information was available on the origin of the Sigma proteins.

Determination of Protein Concentrations. FcRn and IgG concentrations were determined spectrophotometrically using extinction coefficients at 280 nm of 84 900 M^{-1} cm^{-1} (FcRn) and 224 000 M^{-1} cm^{-1} (human IgG). Extinction coefficients were calculated on the basis of the amino acid composition (*21*).

Crystallization, Data Collection, and Processing. Crystals (space group $P4_32_12$; one molecule per asymmetric unit) of hFcRn were grown at 22 °C in 1:1 hanging drops containing FcRn (21 mg/mL) and 1.5 M ammonium sulfate, 100 mM Tris, pH 8.5, and 12% (w/v) glycerol. After noticing that unnucleated drops formed crystals when a tray was left in a warm room, we determined that equilibrated drops (which only rarely nucleated at 22 °C) could be reproducibly nucleated by brief heating (37 °C for 15 min). The pH of the equilibrated drop is estimated to be 8.2, based upon measurement of a mock solution. Crystals with similar unit cell constants have also been grown from a pH 6.8 crystallization buffer, suggesting that the oligomerization state in the crystals does not change between pH 6.8 and pH 8.2. Data were collected at room temperature from a single crystal to 2.7 Å with an R-AXIS II detector using Cu Kα radiation from a Rigaku RU-200 rotating anode (Table 1). Data were processed and scaled with DENZO and SCALEPACK (*22*).

Table 1: Data Collection and Refinement Statistics for hFcRn

space group	$P4_32_12$
unit cell dimensions (Å)	66.4, 66.4, 221.8
data collection	
resolution	30–2.7 (2.8–2.7)
temperature	22 °C
mosaicity	0.21°
observations	79025
unique reflections	14243 (1374)
completeness (%)	98.7 (99.4)
I/σ	23.5 (5.7)
R_{sym} (%)	6.7 (30.7)
refinement	
resolution (Å)	30–2.7
work reflections	13521
test reflections	722 (5%)
R_{cryst} (%)	19.7
R_{free} (%)	24.7
no. of protein atoms	2756 (354 of 366 residues)
no. of water atoms	47
average B factor	55.4 Å^2
anisotropic B correction	$B_{11} = B_{22} = 4.64$ Å^2, $B_{33} = -9.28$ Å^2
model geometry	
rms deviations from ideal	
bond lengths (Å)	0.007
bond angles (deg)	1.3
Ramachandran plot quality	
most favored	87.5%
additionally allowed	11.8%
generously allowed	0.7%
disallowed	0.0%

Structure Solution and Refinement. The structure was determined by molecular replacement using AMoRe (*23*) with the 2.2 Å structure of rFcRn (PDB code 1FRU, nonconserved residues truncated to alanine) as a search model. The top rotation function (20–4 Å) peak yielded a $P4_32_12$ translation function (8–4 Å) solution (correlation coefficient of 30.5%; R factor of 51.6%), which was better than any solution in space group $P4_12_12$, and an electron density map calculated with the $P4_32_12$ solution was interpretable. Rigid body refinement (20–4 Å) resulted in an R_{cryst} of 48.6%. Solvent-flattened maps calculated to 3.0 Å were used for initial rebuilding. Anisotropy and bulk solvent corrections were applied, and the model was refined (30–2.7 Å) using individual temperature (B) factors with X-PLOR (*24*). All structure factors greater than or equal to 0 were used in the refinement. Residues 1–3 and 52–59 of the FcRn heavy chain are not seen in the electron density and have been omitted from the model, and 19 side chains are disordered and were modeled as alanines (FcRn residues 63, 85, 164, 168, 169, 171, 175, 215, and 223; β2m residues 16, 19, 42, 47, 48, 73, 74, 75, 97, and 98). In contrast to the rFcRn structure, in which cysteines in the α2 domain (Cys 98 and Cys 161) existed in alternate conformations (20% in a covalent interaction to form a disulfide bridge; 80% in a noncovalent conformation) (*12*), the counterpart cysteines in hFcRn (Cys 96 and Cys 159) in hFcRn appear completely in the covalent conformation. No carbohydrate is visible at the only potential N-linked glycosylation site, Asn 102, in hFcRn. As in rFcRn, the unpaired cysteine at position 48 appears to be blocked by an unidentified group, which has been modeled as a mercaptoethanol molecule. Figures 2–4 were made with Molscript (*25*) and Raster3D (*26*).

Equilibrium Gel Filtration. The equilibrium column chromatography method of Hummel and Dreyer (*27*) including Scatchard analysis (*28*) was used to analyze the association

of hFcRn with human IgG. Chromatography was performed at a flow rate of 0.1 mL/min using a SMART micropurification system (Pharmacia), and the absorbance of the eluant was monitored at 280 nm. A Superdex 200 PC 3.2/30 gel filtration column was equilibrated with and run in 20 mM sodium phosphate, pH 6.0, and 150 mM NaCl containing 0.25, 0.5, 1.0, 2.5, or 5 μM FcRn (equilibration buffer). Samples (20 μL) including pooled human IgG (not fractionated by subclasses) and various concentrations of FcRn were incubated for 20 min at room temperature in equilibration buffer. At each concentration of FcRn in the equilibration buffer, a series of injections containing a mixture of a fixed concentration of human IgG with a series of FcRn concentrations were performed. Relative trough and peak areas were determined by integrating the FcRn elution region using the SMART system software. By plotting the area of the trough or peak versus the injected FcRn concentration, one can derive the concentration of injected FcRn that would give a flat baseline with no peak or trough at the position where free FcRn elutes. At this injected FcRn concentration, the concentration of free FcRn is equal to that in the equilibration buffer. The concentration of bound FcRn can be determined by subtracting the equilibrium buffer concentration from this injection concentration. Thus, each series of injections at a single equilibration buffer concentration gives one data point (FcRn bound, FcRn bound/FcRn free) for a Scatchard analysis. To maximize the peak or trough signal without excessively depleting the equilibration buffer surrounding the injection volume, we chose the fixed concentration of IgG used for each series of injections to be the same as the FcRn concentration in the equilibration buffer. Hence, the bound term in the Scatchard analysis is normalized as micromoles of FcRn bound per micromole of IgG injected.

Biosensor Assays. A Biacore 2000 biosensor system (Pharmacia, LKB Biotechnology) was used to assay the interaction of FcRn with the different human IgG subclasses. This system includes a biosensor chip with a dextran-coated gold surface to which one protein (referred to as the "ligand") is covalently immobilized. Binding of an injected protein (the "analyte") to the immobilized protein results in changes of the surface plasmon resonance that are directly proportional to the amount of bound protein and read out in real time as resonance units (RU) (*29, 30*). Since each polypeptide chain of an Fc homodimer can be bound by an FcRn molecule (*31*), the observed binding of IgG to immobilized FcRn involves a mixture of singly or doubly liganded Fc regions. At a sufficiently low coupling density of FcRn, interactions involving singly liganded Fc regions predominate. As the coupling density increases, the likelihood of doubly liganded binding increases. When IgG or Fc is immobilized and FcRn is injected, interactions corresponding to the singly liganded population are observed, resulting in a systematically lower apparent affinity than derived when FcRn is immobilized (*31, 32*).

Since we were comparing the binding of a number of different ligands (human IgG subclasses) to a single receptor (hFcRn), affinity measurements were done using immobilized hFcRn and injected human IgG's. hFcRn was covalently immobilized to three of the four flow cells on a CM5 biosensor chip (Pharmacia) using standard primary amine coupling chemistry (Biacore manual) at three different densities (~100, 500–600, and 1000–2500 RU). The fourth

flow cell was mock coupled using buffer to serve as a blank. Human IgG proteins were injected at room temperature in 50 mM sodium phosphate, pH 6.0, and 150 mM NaCl. Binding reactions were allowed to closely approach or to reach equilibrium and K_D's were derived by nonlinear regression analysis of plots of R_{eq} (the equilibrium binding response) versus the analyte concentration. Binding data were fit to a model with two classes of noninteracting binding sites as described for the analysis of rFcRn with IgG (*32*). This model assumes that there are two classes of Fc binding sites on the chip and derives macroscopic equilibrium dissociation constants (K_{D1} and K_{D2}) and the percentage of the total response due to each class of binding sites (f_1 and f_2). The higher affinity binding constant (K_{D1}) corresponds to the affinities measured in cell binding assays involving membrane-bound FcRn (*33, 34*), in which the signal due to lower affinity binding is presumably lost during washing (*32*).

To derive a K_D that corresponds directly to solution-phase affinity measurements, we also analyzed the biosensor data using a bivalent analyte model. The bivalent analyte model fits the binding data to sequential reactions (FcRn + Fc ⇌ FcRn−Fc and FcRn−Fc + FcRn ⇌ FcRn−Fc−FcRn), deriving microscopic K_D's ($K_{D,1st}$ and $K_{D,2nd}$) that correspond to the affinities observed when immobilized IgG interacts with injected FcRn (Figure 6 legend) or when Fc and FcRn interact in solution (Figure 5). For these analyses, we simultaneously fit equilibrium data from flow cells coupled to densities of ~100, 500, and 1500 RU for two K_D's and three coupling densities. The expression for the equilibrium binding response, R_{eq}, for a bivalent analyte is

$$R_{eq} = \frac{SC}{2} + \frac{SK_{D,2nd}}{8}\left(\frac{[A]}{K_{D,1st}} - \frac{K_{D,1st}}{[A]}\right) \times \left(\sqrt{1 + \frac{8CK_{D,1st}[A]}{K_{D,2nd}(K_{D,1st} + [A])^2}} - 1\right)$$

where R_{eq} is the equilibrium response in resonance units (RU), C is the coupling density of the ligand (FcRn) in moles per liter, [A] is the concentration of the analyte (IgG), and S is a scale factor (resonance units per mole per liter of analyte). From the above expression for R_{eq}, one can show that half of the maximal response occurs when [A] = $K_{D,1st}$ and that half of the ligand molecules are bound to analyte when [A] = $K_{D,1st}K_{D,2nd}/(K_{D,2nd} + C)$, which is equivalent to K_{D1}, the macroscopic high-affinity binding constant. When the coupling density concentration, C, is comparable to $K_{D,2nd}$, the macroscopic affinity becomes dependent on the coupling density due to an avidity effect. For a related discussion in the context of bivalent antibody interactions with antigens, see ref *35*.

RESULTS

Overview of the hFcRn Crystal Structure. Soluble hFcRn was expressed in CHO cells and purified using the pH-dependent Fc binding activity that hFcRn shares with the rodent forms of FcRn. The crystal structure of hFcRn was determined to 2.7 Å by molecular replacement using the 2.2 Å structure of rFcRn (*12*). The overall structure of hFcRn

closely resembles that of rFcRn, both having an MHC class I-like fold (Figure 2). The heavy chains of FcRn and class I MHC molecules are composed of an α1−α2 superdomain containing an eight-stranded antiparallel β-sheet topped by two α-helices, which is linked to the immunoglobulin-like α3 domain. The β2m light chain interacts with the heavy chains of rFcRn, hFcRn, and class I MHC proteins in a similar manner, making contacts with the underside of the α1−α2 platform and with the side of the α3 domain (Figure 2A).

The loop immediately preceding the α1 domain helix (residues 52−59) is disordered in the hFcRn structure, although it is ordered in the rFcRn structures (*12, 15*). This loop contains two partially solvent-exposed tryptophan residues (Trp 53 and Trp 59) that are conserved in all known FcRn sequences (Figure 1), though they are not present in class I MHC proteins or other class I homologues. These tryptophans have no clear structural role in FcRn and are on the opposite face of the α1−α2 platform from the Fc binding site (*13*). Exposure to solvent and being disordered in the hFcRn structure is consistent with a role other than maintaining the structure of FcRn. One possible function for these residues is to interact with the membrane bilayer to facilitate orientation of FcRn in a "lying down" conformation on the membrane (*12, 13*), thereby exposing the Fc binding site in a orientation that minimizes steric hindrance for binding IgG. Such tryptophan−membrane interactions have been proposed for other cell surface proteins, for example, myelin protein P_0 (*36*).

The most notable structural difference between FcRn and MHC class I proteins is the absence of a functional peptide binding groove in FcRn. Structural features of rFcRn that result in groove closure and the inability to bind peptides include (1) the side chain of Arg 164, which occludes the rFcRn counterpart of the class I MHC pocket that interacts with main-chain atoms of the peptide N-terminus (pocket A), and (2) a kink in the α2 domain helix near rFcRn Pro 162, which is associated with an almost rigid body displacement of a 40-residue region (residues 121−161) encompassing the N-terminal portion of the α2 helix, the preceding short helix, and the two outermost strands of the α2 β-sheet (*12*). These groove closure features are also found in hFcRn (Figure 2B). We originally suggested that the rearrangement in the α2 domain helix results from the presence of a helix-breaking residue (Pro 162 in rFcRn, Pro 160 in hFcRn) (*12*). Another class I MHC homologue, CD1, includes an analogous proline positioned near a kink in its α2 domain helix (*37*), whereas the analogous residue in class I MHC molecules is a valine (*38*). However, two recent structures of class I MHC homologues [HFE (*39*) and ZAG (*40*)] reveal α2 domain helices that accommodate a proline at this position without distortion compared to the α2 domain helices in class I MHC molecules. Hence, features in addition to the proline in the α2 domain helix must contribute to groove closure in FcRn. By identifying structural features common to hFcRn and rFcRn, we can locate residues likely to be involved in closure of the FcRn groove. In both FcRn structures, the position of the α2 domain helix is stabilized by close contact between residues on the α1 and α2 domain helices, thereby closing off the right side (as depicted in Figure 2B) of the groove. Conserved interactions between the α1 and α2 domain helices (*15*) include a salt bridge
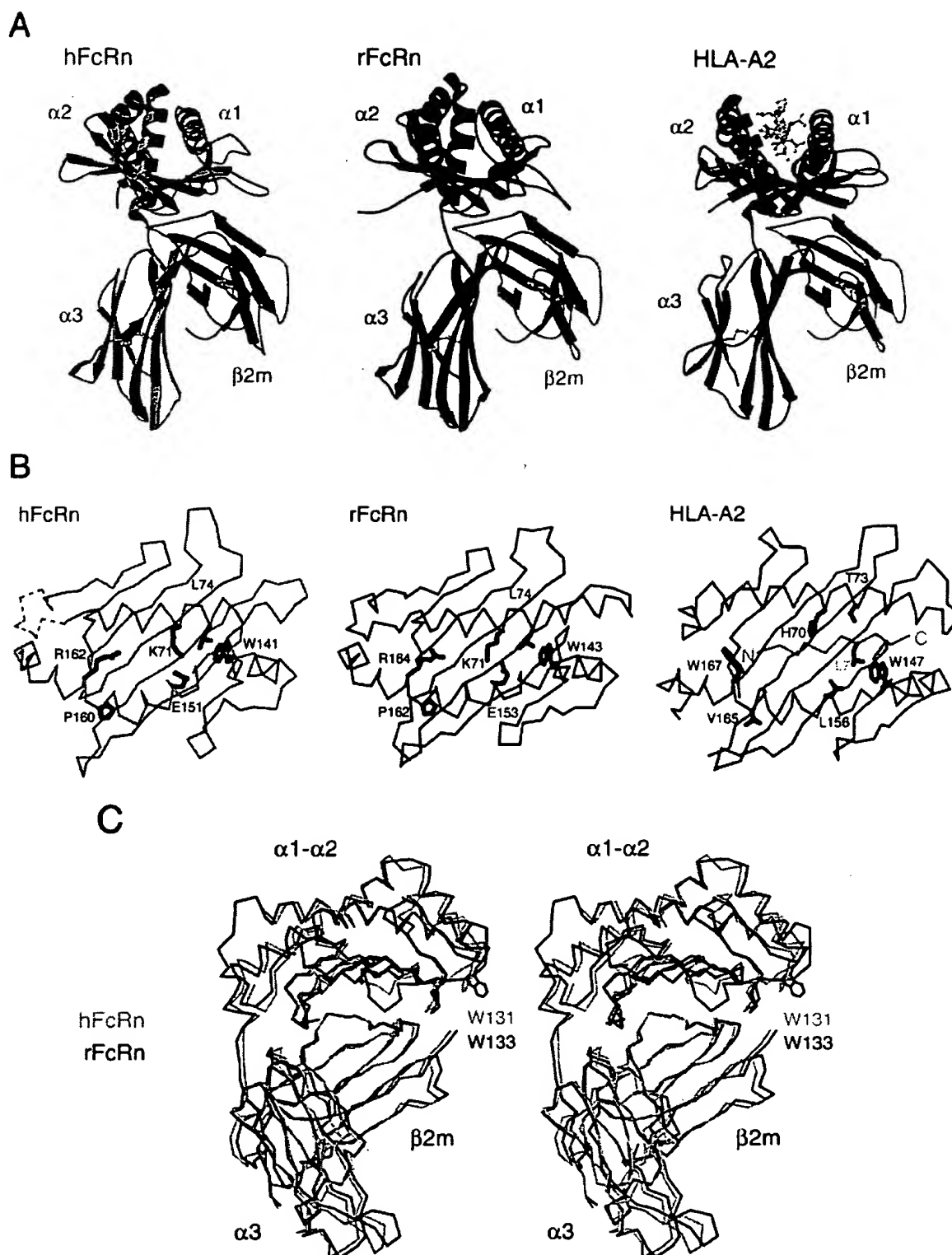
A

B

C

FIGURE 2: (A) Ribbon diagrams of hFcRn, rFcRn (PDB code 3FRU), and the class I MHC molecule HLA-A2 [PDB code 2CLR (57)]. (B) Comparisons of the grooves of hFcRn, rFcRn, and HLA-A2. The disordered loop in hFcRn (residues 52−59) is shown as a dashed line using the rFcRn structure in this region. (C) Stereo overlay of the hFcRn and rFcRn structures after superposition of Cα atoms in the α1−α2 platform. A key residue at the Fc binding site (42) (rFcRn Trp 133; hFcRn Trp 131) is highlighted on each structure. Root-mean-square deviations between hFcRn and rFcRn: overall, 1.09 Å (344 Cα atoms); α1 domain, 1.09 Å (69 Cα atoms); α2 domain, 1.15 Å (83 Cα atoms); α3 domain, 0.72 Å (90 Cα atoms); β2m, 0.67 Å (99 Cα atoms).

between Lys 71 and Glu 151 (rFcRn Glu 153) and a hydrophobic contact between Leu 74 and Trp 141 (rFcRn Trp 143). In both forms of FcRn, the side chain of Leu 74 occludes a region analogous to a pocket (pocket E) that accepts a side chain from the bound peptide in class I MHC molecules.
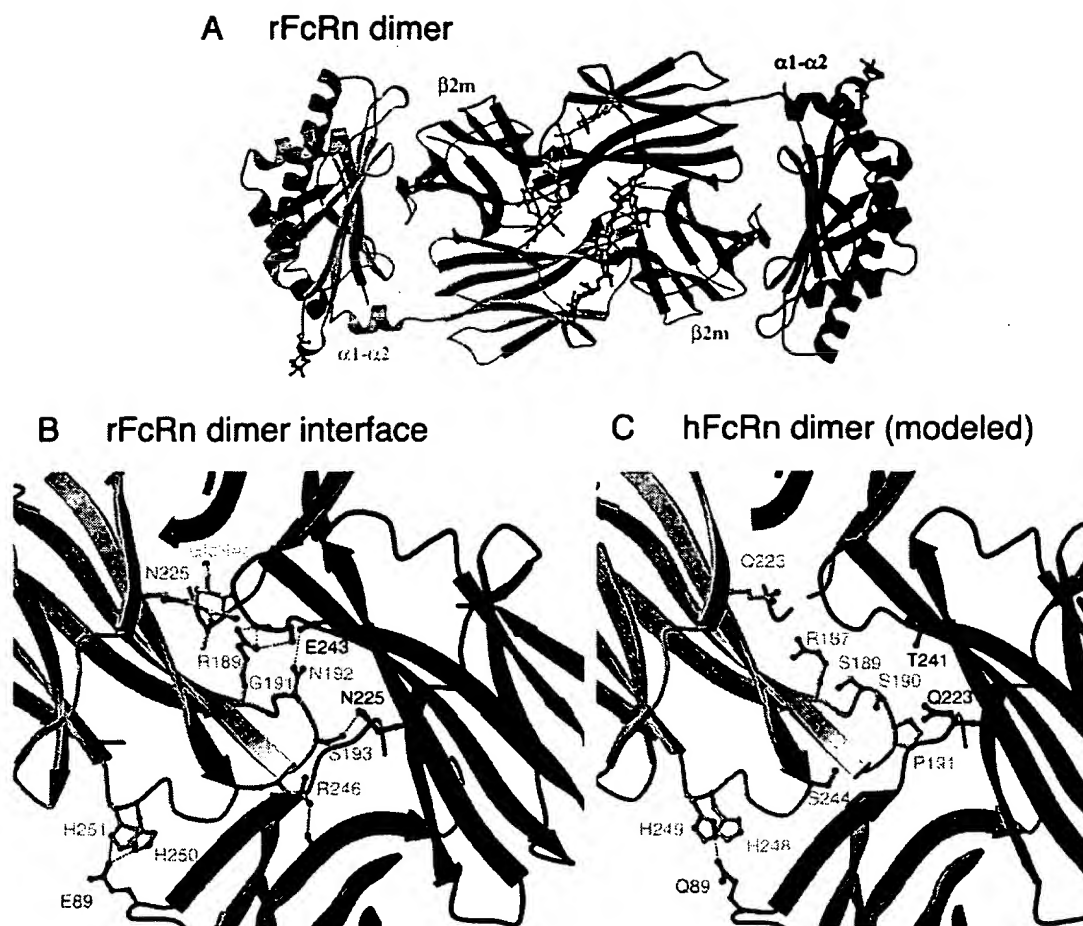
FIGURE 3: Comparison of the rFcRn dimer interface with a hypothetical hFcRn dimer interface. (A) Ribbon diagram of the rFcRn dimer (PDB entry 3FRU) including ordered carbohydrate residues. The ordered carbohydrate of each rFcRn heavy chain interacts extensively with the α3 domain of the dimer-related molecule. (B) Close-up view of the rFcRn dimer interface. Side chains are displayed if an atom from the residue is within 3.5 Å of a residue on the other molecule. For clarity, each such residue is shown only on one of the dimer-related molecules, and only the sugar residue directly attached to Asn 225 is shown. (C) Model of a hypothetical hFcRn dimer derived from the crystallographically observed rFcRn dimer by aligning the α3 domains of two hFcRn molecules with the rFcRn α3 domains.

hFcRn Does Not Form Dimers in the Crystals. A distinctive feature of rFcRn crystals is the presence of dimers of rFcRn heterodimers. The same 2-fold symmetric dimers, mediated by contacts between the α3 and β2m domains (Figure 3A), were present as noncrystallographically related partners in three different crystal forms of rFcRn (space groups $C222_1$, $P2_1$, and $P3_121$) (*12*) and as a crystallographically related dimer in the FcRn–Fc cocrystals (*13*). It was suggested that the rFcRn dimer represents a dimer normally induced by IgG binding and that the high protein concentrations required for crystallization permitted formation of the dimer in the absence of IgG (*12–14*). Since the $C222_1$ crystal form, which contains three rFcRn molecules per asymmetric unit, includes an rFcRn monomer along with an rFcRn dimer, dimerization is favored but not obligatory in rFcRn crystals. Dimerization of rFcRn is mediated by electrostatic interactions and ordered carbohydrate residues attached to Asn 225 (*15*) (Figure 3A). A total of 2600 Å² of surface area is buried at the rFcRn dimer interface, of which 1500 Å² is buried by protein–protein interactions and 1100 Å² is buried by interactions between the ordered carbohydrate and protein components of the dimer-related molecule (*15*). The interactions of α3 domain residues His 250 and His 251 with Glu

89 of the dimer-related β2m, and Gly 191 with its counterpart on the dimer-related molecule, were previously examined by site-directed mutagenesis. Mutation of rFcRn His 250 and His 251 resulted in a 6-fold reduction in affinity between rFcRn and IgG (*41*), and substitution of β2m Glu 89 reduced the binding affinity by 3–4-fold (*42*), although these residues are distant from the Fc binding site (*13*). Likewise, substitution of Gly 191 with a residue containing a larger side chain resulted in a 3–9-fold affinity reduction (*42*). These results suggest that rFcRn dimerization is required to achieve maximal binding affinity for IgG.

In contrast to the rFcRn crystal forms, hFcRn does not form dimers in the one crystal form that was obtained. This crystal form (space group $P4_32_12$) contains one hFcRn heterodimer per asymmetric unit and does not include hFcRn dimers related by crystallographic symmetry. To address the possibility of forming hFcRn dimers, we generated a model of an hFcRn dimer (Figure 3C) based upon the structure of the rFcRn dimer (Figure 3A,B). Although hFcRn molecules can be accommodated in a dimer without significant steric difficulties, several features of the rFcRn dimer interface are not conserved in an hFcRn dimer. First, there can be no carbohydrate–protein interactions at an hFcRn dimer inter-
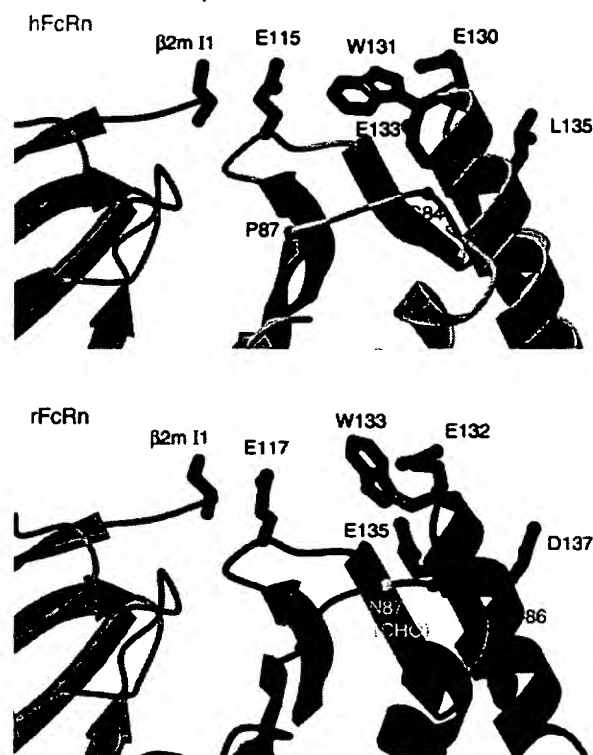
FIGURE 4: Comparison of the Fc binding site. Residues identified as part of the rFcRn binding site for Fc, as predicted by the low-resolution rFcRn—Fc cocrystal structure (*13*) and confirmed by site-directed mutagenesis (*42*), are highlighted on the structures of rFcRn and hFcRn. rFcRn residues 84—86 are in the vicinity of the Fc binding site, but substitution of these residues for their class I MHC counterparts results in no change in the affinity between rFcRn and IgG (*42*). The loop containing rFcRn residues 84—86 differs between hFcRn and rFcRn in that the hFcRn loop is two residues shorter (Figure 1), does not contain an N-linked glycosylation attachment site (indicated on the rFcRn structure at residue 87), and includes a *cis*-proline at residue 87.

face because the potential N-linked glycosylation site is lost in hFcRn by the replacement of Asn 225 in rFcRn by a glutamine in hFcRn (Gln 223). Other interactions favorable for dimer formation in rFcRn are not possible in an hFcRn dimer, including (1) the electrostatic interaction between His 250 and His 251 (hFcRn His 248 and His 249) and β2m Glu 89 and (2) the hydrogen bonds from Arg 246 (rFcRn numbering) to Ile 7 of the partner β2m and from Asn 192 and Ser 193 to Glu 243 and Asn 225, respectively, of the dimer-related α3 domain (Figure 3B,C). These differences may explain the propensity of rFcRn to dimerize in crystals compared with hFcRn, but further studies will be required to assess whether FcRn of either species dimerizes on membranes.

Comparison of the Fc Binding Interface on hFcRn and rFcRn. In earlier studies, residues at the rFcRn binding site for Fc were predicted from the low-resolution FcRn—Fc cocrystal structure (*13*) and tested for their effects on Fc binding by site-directed mutagenesis (*42*). Residues with significant effects on the affinity between rFcRn and IgG are highlighted on the rFcRn and hFcRn structures in Figure 4. Although the binding site is generally conserved between the two receptors, there are three notable differences between the hFcRn and rFcRn structures in this region. First, Trp

131 in hFcRn packs against the Cβ atom of Phe 117 and is thus less solvent exposed than its rat counterpart, Trp 133. This tryptophan is thought to interact with a hydrophobic patch on Fc that includes Ile 253, which was identified as a critical residue on Fc for interaction with FcRn (*43—47*). Since the tryptophan side chain is not constrained into any particular conformation in uncomplexed hFcRn or rFcRn, it may adopt a different conformation upon binding Fc. Another difference in the Fc binding site is the replacement of Asp 137 of rFcRn by Leu 135 in hFcRn. The FcRn—Fc cocrystal structure predicts that Asp 137 is in the vicinity of Fc His 435 (*13*), suggesting that it might participate in a pH-dependent electrostatic interaction in the rFcRn—IgG complex, consistent with the observation that substitution of Asp 137 to an asparagine reduces the affinity of rFcRn for IgG by >8000-fold (*42*). Since Fc residue 435 is not conserved as a histidine in all species and subclasses of IgG (*38*), hFcRn and rFcRn are predicted to recognize IgG's with different rank order affinities. The third difference in the vicinity of the Fc binding site between hFcRn and rFcRn results from the two-residue deletion in hFcRn at the C-terminal end of the α1 domain helix (Figure 4). The structural manifestation of this difference is the deletion of about one turn of that helix. The loop connecting this end of the helix to the α1—α2 platform also differs from its counterpart in rFcRn, because it lacks a potential N-linked carbohydrate site present at Asn 87 in rFcRn and includes a *cis*-proline (hFcRn Pro 87). Although this loop is predicted to be in the vicinity of an IgG ligand on the basis of the low-resolution FcRn—Fc complex structure (*13*), replacement of part of this region of rFcRn (residues 84—86, without disruption of the N-linked glycosylation site at Asn 87) with the corresponding MHC class I residues had no effect on IgG binding (*42*).

Stoichiometry of the hFcRn—IgG Complex. To determine the stoichiometry of the hFcRn—IgG interaction, we performed a series of equilibrium gel filtration experiments. Conventional gel filtration experiments are often used to assess the stoichiometry of protein complexes. However, transient dissociation of weak complexes during chromatography can lead to altered stoichiometries (*17*). To avoid this problem, gel filtration experiments can be done under equilibrium conditions by including one of the binding partners in the running buffer (*27*), as described for previous studies of rFcRn and mFcRn (*17, 31*). For our experiments, the gel filtration column is equilibrated and run using a buffer containing a fixed concentration of hFcRn (the equilibration buffer). Different ratios of hFcRn plus IgG are then injected onto the column in equilibration buffer. Although transient dissociation of hFcRn—IgG complexes occurs at the same rate as in a conventional gel filtration experiment, hFcRn that dissociates from a complex can be replaced by hFcRn in the equilibration buffer. For each concentration of hFcRn in the equilibration buffer, there is a ratio of injected proteins such that no peak or trough appears at the elution volume of free FcRn (Figure 5A). By determining this ratio at several concentrations of FcRn in the equilibration buffer, one can perform a Scatchard analysis yielding both a stoichiometry and a solution-phase affinity (*28*). The Scatchard analysis in Figure 5B shows an *x*-intercept of 1.92; thus, the stoichiometry of the hFcRn—IgG complex is 2:1 (two molecules of hFcRn bind to each IgG), in agreement with
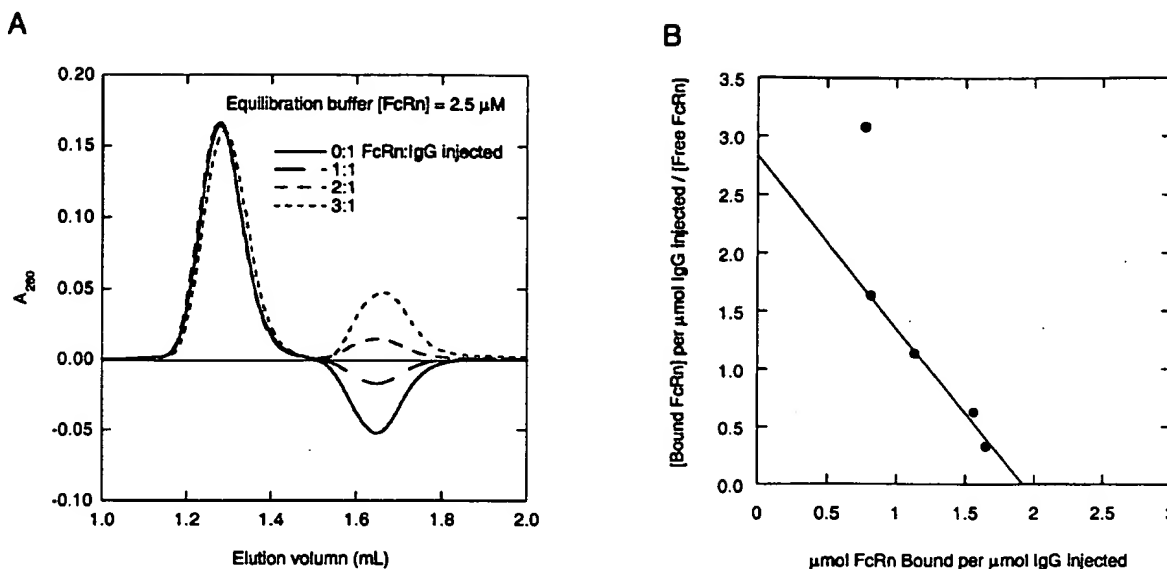
A

B

FIGURE 5: Equilibrium gel filtration analyses of hFcRn—IgG complexes. (A) hFcRn was incubated with 2.5 μM IgG in the presence of 0, 1, 2, or 3 (additional) equiv of hFcRn in a buffer containing 2.5 μM hFcRn (equilibration buffer). Samples were then injected onto a column equilibrated in the equilibration buffer. The peak that elutes first corresponds to an FcRn—IgG complex. The second peak or trough is at the elution volume of free FcRn (~1.65 mL). From this series of injections, one can calculate the FcRn concentration that, when co-injected with 2.5 μM IgG, yields a free FcRn concentration of 2.5 μM (i.e., no FcRn peak/trough). The above series of injections were repeated with equilibration buffers containing 0.25, 0.5, 1.0, and 5.0 μM FcRn concentrations (data not shown). (B) Scatchard plot including data from equilibration buffers containing 0.25, 0.5, 1.0, 2.5, and 5.0 μM FcRn. The data point derived from the lowest FcRn concentration (0.25 μM) does not fall on the best-fit line to the higher concentration data. Because the absorbance of this sample was relatively small, a sizable baseline drift may have disturbed this measurement. The best-fit line to the data derived from the four highest concentrations yields a K_D of 700 nM and an x-intercept of 1.92.

previous studies of rFcRn and mFcRn (*17*). The calculated affinity of 700 nM is comparable to that obtained for rFcRn by another solution-phase measurement, isothermal titration calorimetry, which derived a 500 nM binding constant between rFcRn and human IgG1 (*16*).

Binding Affinities between hFcRn and Human IgG Subclasses. To investigate the subclass binding specificity of hFcRn, we performed a series of affinity measurements using an SPR assay. hFcRn was covalently immobilized onto a biosensor chip, and the binding of various purified human IgG proteins was monitored by the change in the SPR signal, as previously described (*32*). An earlier binding study involving rFcRn noted affinity differences between antibodies of the same subclass (*47*), suggesting that allotypic variations within a single subclass of IgG may affect the affinity for FcRn. To check for possible effects of allotypic differences among human IgG's upon binding hFcRn, two independent commercial sources of purified human IgG subclasses were used (set 1 and set 2; Figure 6B).

For each antibody evaluated, a series of injections containing 1 nM—10 μM IgG were allowed to reach or nearly reach equilibrium. These data were fit by nonlinear regression analysis to derive two equilibrium dissociation constants, K_{D1} and K_{D2}, along with their fractional occupancies, f_1 and f_2 (Figure 6). For the high-affinity population, which generally accounted for a majority of the binding response, the K_D (K_{D1}) ranged from 9 to 69 nM, while the low-affinity population ranged in K_D from 470 to 1250 nM. These affinities are comparable to those obtained for rFcRn binding to mouse and rat IgG subclasses under similar conditions, where K_{D1} ranged from 15 to 93 nM (*32*), but are somewhat higher affinity than the 160 nM K_D derived for the interaction

of radiolabeled human IgG with hFcRn in microvillous membranes from human fetal intestine (*34*).

The binding affinities presented in Figure 6B demonstrate that affinity differences due to allotypic variations within a single subclass of human IgG are comparable to differences between the subclasses. For example, in IgG set 1, the highest affinity subclass is IgG2 and the lowest affinity subclass is IgG3, whereas in IgG set 2, IgG3 binds most strongly, IgG2 is intermediate, and IgG4 binds with the lowest affinity. Since two different rank orderings of the affinities for the different subclasses are derived using different sources of human IgG, hFcRn does not show clear subclass preferences for binding of human IgG. Allotypic variations within individual human IgG subclasses provide a plausible explanation for the different rank orderings of the affinities. The IgG3 allotypes G3m(b), G3m(g), and G3m(s,t) correspond to amino acid changes at positions 379, 384, 392, 397, 435, and 436 (*48*). Two of these positions, 435 and 436, are predicted to be at the rFcRn—Fc interface (*13*), and recombinant Fc's with mutations at these sites have altered affinities for mFcRn and increased catabolic rates in mice (*46*). The common IgG3 allotypes have arginine at position 435, while the relatively uncommon G3m(s,t) IgG3 allotype has a histidine at position 435. The substitution of His 435 for arginine has been suggested to be responsible for the short serum half-life of human IgG3, and a recombinant human Fc derived from IgG1 with this mutation has a reduced half-life in mice (*49*). Allotypes G3m(b) and G3m(g) have tyrosine and phenylalanine, respectively, at position 436 (*48*). In most rodent IgG subclasses, position 436 is a histidine, which is believed to interact with an acidic residue on rFcRn (*13, 15*). Since allotypic differences occur in Fc residues predicted to interact

A   IgG Set 1   IgG Set 2

B

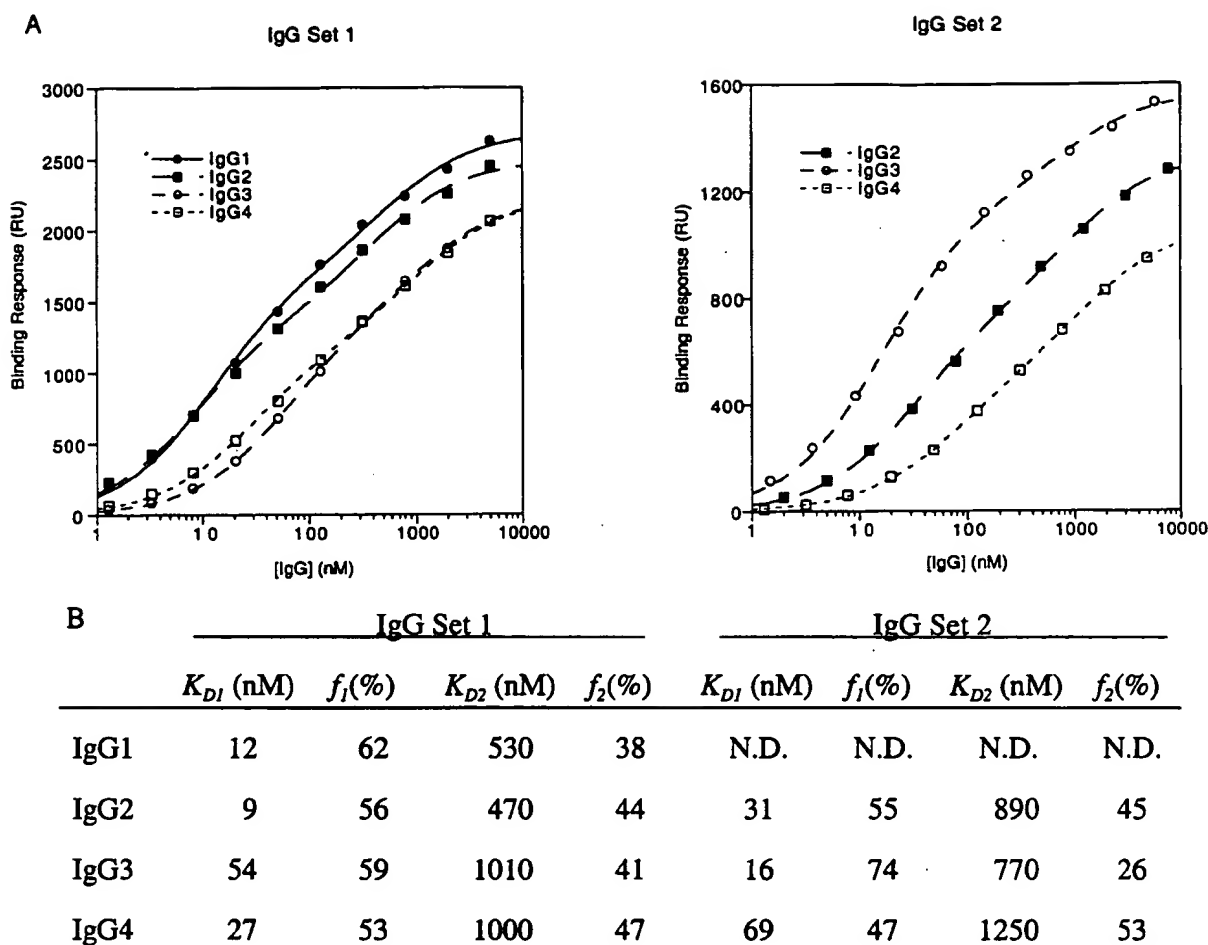|	IgG Set 1				IgG Set 2			
	K_{D1} (nM)	f_1(%)	K_{D2} (nM)	f_2(%)	K_{D1} (nM)	f_1(%)	K_{D2} (nM)	f_2(%)
IgG1	12	62	530	38	N.D.	N.D.	N.D.	N.D.
IgG2	9	56	470	44	31	55	890	45
IgG3	54	59	1010	41	16	74	770	26
IgG4	27	53	1000	47	69	47	1250	53

FIGURE 6: Biosensor analyses of hFcRn interacting with human IgG's. (A) Equilibrium binding of human IgG subclasses to hFcRn immobilized on a biosensor chip is plotted as a function of the log of the IgG concentration. Best-fit binding curves, modeled as two classes of noninteracting binding sites, are superimposed on the binding data. IgG set 1 corresponds to human myeloma proteins purchased from Calbiochem injected over hFcRn coupled at a density of 2600 RU. IgG set 2 corresponds to human myeloma proteins purchased from Sigma injected over hFcRn coupled at a density of 1000 RU. (B) Binding affinities derived from the data in panel A. Analyses of data from a lower hFcRn coupling density (500−600 RU) yield K_D's that are consistently about 2-fold higher, but the rank order of affinities within each set is the same at both coupling densities. Analyses of the same equilibrium binding data using a bivalent analyte model (Materials and Methods) yields a binding affinity of 1−2 μM for all subclasses. This value is similar to that obtained by gel filtration (Figure 5) and to the affinity observed when IgG is immobilized and hFcRn is flowed over the biosensor chip ($K_{D1} = 1.1$ μM with IgG2 immobilized; data not shown).

with FcRn, the different rank orders for the IgG3 affinities in IgG sets 1 and 2 could result from use of different IgG3 allotypes.

DISCUSSION

FcRn functions by transporting IgG across epithelial cells and by rescuing IgG from protein catabolism (*1−3*). These activities result from the binding of FcRn to the Fc portion of IgG within acidic intracellular compartments and release of IgG upon exposure to the slightly basic pH of the bloodstream. With the continuing research and development of antibodies and antibody chimeric proteins as potential therapeutic agents in humans (reviewed in refs *50* and *51*), detailed knowledge of the interaction between hFcRn and IgG may be useful for drug design. Alteration of natural Fc domains to increase their affinity for FcRn has been demonstrated as a means of increasing the serum half-life of antibodies (*52*). This may be of benefit for the development of antibody-based drugs, particularly since the long-

sought goal of developing specific immunoglobulin agents as cancer treatments is beginning to yield clinically useful drugs (e.g., anti-HER2 for breast cancer and anti-CD20 for non-Hodgkin's lymphoma) (*51*).

For one class of immunoglobulin agents, immunotoxins, the benefits of altering Fc regions to facilitate interaction with FcRn might extend beyond increasing serum persistence to improved therapeutic indices. An immunotoxin consists of a variable domain specific for a tumor marker conjugated to a highly active toxin, such as the ricin A chain or diphtheria toxin (*53*). The dose-limiting toxic effect of many potential immunotoxin therapies is vascular leak syndrome (*53*), which occurs when blood vessels become too permeable, leading to edema and hypoalbuminemia, among other signs. Although the etiology of vascular leak syndrome is complex, a portion is due to toxin-mediated death of vascular endothelial cells (*54*), which line the interior surface of blood vessels. The predominant expression site of FcRn in the adult is the vascular endothelium, which is also the primary site

of plasma protein catabolism (2). Since endocytosis of the immunotoxin is an early event in the action of these agents, improved interactions with FcRn might reduce immunotoxin-associated toxicity to endothelial cells by diverting more of the conjugates back to the cell surface.

To facilitate understanding of how to modify the interactions of human IgG with hFcRn, we have determined the crystal structure of hFcRn and examined the stoichiometry, affinity, and subclass specificity of the hFcRn—IgG interaction. The structure of hFcRn is similar to the previously determined structure of rFcRn (12). Both forms of FcRn share a common fold with class I MHC molecules but do not have functional peptide binding grooves. Crystals of hFcRn do not contain the dimer of FcRn heterodimers observed in crystals of rFcRn alone and rFcRn complexed with Fc (12, 13). The absence of dimerization in crystallized hFcRn is consistent with the lack of conservation of residues and an ordered N-linked carbohydrate that mediate dimerization in rFcRn (15). rFcRn appears monomeric in solution (20); thus, one interpretation of the crystallographically observed dimers of rFcRn is that rFcRn has a weak tendency to dimerize, which is enhanced by binding to Fc. Further studies will be necessary to determine whether hFcRn dimerizes in vivo in the presence of IgG. In addition to the structural studies of hFcRn, we also characterized the interaction between hFcRn and human IgG. Using equilibrium gel filtration, we find a 2:1 hFcRn:IgG binding stoichiometry, as also observed for the interactions of IgG with rFcRn and mFcRn (16, 17). Binding affinities derived using a biosensor-based assay between immobilized hFcRn and human IgG are also comparable to those derived for rFcRn interactions with IgG under similar conditions (32).

Understanding the relationship between subclass and allotype structural features, their affinities for FcRn, and their half-lives may permit rational design of antibody reagents with increased serum persistence. The effect of human IgG structure on antibody catabolism is reflected in the half-lives of the four subclasses: IgG1, IgG2, and IgG4 each have a 21-day half-life, while the IgG3 subclass has a half-life of 7 days (55). Recent studies of mFcRn have demonstrated a correlation between IgG affinity for mFcRn and serum half-life (49, 52, 56). If the serum half-life of IgG in humans correlates strictly with affinity for hFcRn, we would expect IgG3 to have a lower affinity than the other subclasses. However, when we examined the binding of two sets of human IgG subclasses to hFcRn using a biosensor assay, we did not find systematic differences between the affinity for IgG3 and the affinity for the other subclasses. Instead, we found that all subclasses bind hFcRn with affinities within the same order of magnitude and that allotypic variations between individual subclasses had as great an effect on affinity as differences between subclasses. These results suggest that allotypic variations within human IgG subclasses should be taken into account when comparing the serum persistence of IgG subclasses. In addition, since FcRn interactions with IgG are not at equilibrium in vivo, relative serum half-lives may depend on the kinetics of binding to a finite population of FcRn molecules and thus may not directly correlate with affinity measurements. These results, together with the three-dimensional structure of hFcRn, should be useful in efforts to alter the serum half-lives of human antibodies and, hence, assist in the development of more effective immunoglobulin-based therapeutics.

REFERENCES

1. Ghetie, V., and Ward, E. S. (1997) *Immunol. Today 18*, 592–598.
2. Junghans, R. P. (1997) *Immunol. Res. 16*, 29–57.
3. Simister, N. E., Israel, E. J., Ahouse, J. C., and Story, C. M. (1997) *Biochem. Soc. Trans. 25*, 481–486.
4. Story, C. M., Mikulska, J. E., and Simister, N. E. (1994) *J. Exp. Med. 180*, 2377–2381.
5. Ghetie, V., Hubbard, J. G., Kim, J.-K., Tsen, M.-F., Lee, Y., and Ward, E. S. (1996) *Eur. J. Immunol. 26*, 690–696.
6. Junghans, R. P., and Anderson, C. L. (1996) *Proc. Natl. Acad. Sci. U.S.A. 93*, 5512–5516.
7. Israel, E. J., Wilsker, D. F., Hayes, K. C., Schoenfeld, D., and Simister, N. E. (1996) *Immunology 89*, 573–578.
8. Simister, N. E., and Rees, A. R. (1985) *Eur. J. Immunol. 15*, 733–738.
9. Simister, N. E., and Mostov, K. E. (1989) *Nature 337*, 184–187.
10. Ahouse, J. J., Hagerman, C. L., Mittal, P., Gilbert, D. J., Copeland, N. G., Jenkins, N. A., and Simister, N. E. (1993) *J. Immunol. 151*, 6076–6088.
11. Kacskovics, I., Wu, Z., Simister, N. E., Frenyó, L. V., and Hammarström, L. (2000) *J. Immunol. 164*, 1889–1897.
12. Burmeister, W. P., Gastinel, L. N., Simister, N. E., Blum, M. L., and Bjorkman, P. J. (1994) *Nature 372*, 336–343.
13. Burmeister, W. P., Huber, A. H., and Bjorkman, P. J. (1994) *Nature 372*, 379–383.
14. Raghavan, M., and Bjorkman, P. J. (1996) *Annu. Rev. Cell Biol. 12*, 181–220.
15. Vaughn, D. E., and Bjorkman, P. J. (1998) *Structure 6*, 63–73.
16. Huber, A. H., Kelley, R. F., Gastinel, L. N., and Bjorkman, P. J. (1993) *J. Mol. Biol. 230*, 1077–1083.
17. Sánchez, L. M., Penny, D. M., and Bjorkman, P. J. (1999) *Biochemistry 38*, 9471–9476.
18. Bebbington, C. R., and Hentschel, C. C. G. (1987) in *DNA Cloning: A Practical Approach* (Glover, D. M., Ed.) pp 163–188, IRL Press, Oxford.
19. Fahnestock, M. L., Tamir, I., Narhi, L., and Bjorkman, P. J. (1992) *Science 258*, 1658–1662.
20. Gastinel, L. N., Simister, N. E., and Bjorkman, P. J. (1992) *Proc. Natl. Acad. Sci. U.S.A. 89*, 638–642.
21. Mach, H., Middaugh, C. R., and Lewis, R. V. (1992) *Anal. Biochem. 200*, 74–80.
22. Otwinowski, Z., and Minor, W. (1997) *Methods Enzymol. 276*, 307–326.
23. Navaza, J. (1994) *Acta Crystallogr. A50*, 157–163.
24. Brünger, A. T. (1992) *X-PLOR (Version 3.1): A System for Crystallography and NMR*, Yale University, New Haven, CT.
25. Kraulis, P. J. (1991) *J. Appl. Crystallogr. 24*, 946–950.
26. Merritt, E. A., and Murphy, M. E. P. (1994) *Acta Crystallogr. D50*, 869–873.
27. Hummel, J. P., and Dreyer, W. J. (1962) *Biochim. Biophys. Acta 63*, 530–532.
28. Gegner, J. A., and Dahlquist, F. W. (1991) *Proc. Natl. Acad. Sci. U.S.A. 88*, 750–754.
29. Fägerstam, L. G., Frostell-Karlsson, A., Karlsson, R., Persson, B., and Rönnber, I. (1992) *J. Chromatogr. 597*, 397–410.
30. Malmqvist, M. (1993) *Nature 361*, 186–187.
31. Martin, W. L., and Bjorkman, P. J. (1999) *Biochemistry 38*, 12639–12647.

32. Vaughn, D. E., and Bjorkman, P. J. (1997) *Biochemistry 36*, 9374−9380.

33. Mackenzie, N. (1984) *Immunol. Today 5*, 364−366.

34. Israel, E. J., Simister, N., Freiberg, E., Caplan, A., and Walker, W. A. (1993) *Immunology 79*, 77−81.

35. Junghans, R. P. (1999) *Immunol. Today 20*, 401−406.

36. Shapiro, L., Doyle, J. P., Hensley, P., Colman, D. R., and Hendrickson, W. A. (1996) *Neuron 17*, 435−449.

37. Zeng, Z. H., Castaño, A. R., Segelke, B., Stura, E. A., Peterson, P. A., and Wilson, I. A. (1997) *Science 277*, 339−345.

38. Kabat, E. A., Wu, T. T., Perry, H. M., Gottesman, K. S., and Foeller, C. (1991) *Sequences of proteins of immunological interest*, U.S. Department of Health and Human Services, Bethesda, MD.

39. Lebrón, J. A., Bennett, M. J., Vaughn, D. E., Chirino, A. J., Snow, P. M., Mintier, G. A., Feder, J. N., and Bjorkman, P. J. (1998) *Cell 93*, 111−123.

40. Sánchez, L. M., Chirino, A. J., and Bjorkman, P. J. (1999) *Science 283*, 1914−1919.

41. Raghavan, M., Chen, M. Y., Gastinel, L. N., and Bjorkman, P. J. (1994) *Immunity 1*, 303−315.

42. Vaughn, D. E., Milburn, C. M., Penny, D. M., Martin, W. L., Johnson, J. L., and Bjorkman, P. J. (1997) *J. Mol. Biol. 274*, 597−607.

43. Kim, J.-K., Tsen, M.-F., Ghetie, V., and Ward, E. S. (1994) *Eur. J. Immunol. 24*, 2429−2434.

44. Kim, J.-K., Tsen, M.-F., Ghetie, V., and Ward, E. S. (1994) *Scand. J. Immunol. 40*, 457−465.

45. Kim, J. K., Tsen, M. F., Ghetie, V., and Ward, E. S. (1994) *Eur. J. Immunol. 24*, 542−548.

46. Medesan, C., Matesoi, D., Radu, C., Ghetie, V., and Ward, E. S. (1997) *J. Immunol. 158*, 2211−2217.

47. Raghavan, M., Bonagura, V. R., Morrison, S. L., and Bjorkman, P. J. (1995) *Biochemistry 34*, 14649−14657.

48. Jefferis, R. (1990) in *The Human IgG Subclasses: Molecular analysis of structure, function and regulation* (Shakib, F., Ed.) pp 15−30, Pergamon Press, New York.

49. Kim, J.-K., Firan, M., Radu, C. G., Kim, C.-H., Ghetie, V., and Ward, E. S. (1999) *Eur. J. Immunol. 29*, 2819−2825.

50. Farah, R. A., Clinchy, B., Herrera, L., and Vitetta, E. S. (1998) *Crit. Rev. Eukaryot. Gene Expr. 8*, 321−345.

51. Hudson, P. J. (1999) *Curr. Opin. Immunol. 11*, 548−557.

52. Ghetie, V., Popov, S., Borvak, J., Radu, C., Matesoi, D., Medesan, C., Ober, R. J., and Ward, E. S. (1997) *Nat. Biotechnol. 15*, 637−640.

53. Kreitman, R. J. (1999) *Curr. Opin. Immunol. 11*, 570−578.

54. Lindstrom, A. L., Erlandsen, S. L., Kersey, J. H., and Pennell, C. A. (1997) *Blood 90*, 2323−2334.

55. Waldmann, T. A., and Strober, W. (1969) *Prog. Allergy 13*, 1−110.

56. Medesan, C., Cianga, P., Mummert, M., Stanescu, D., Ghetie, V., and Ward, E. S. (1998) *Eur. J. Immunol. 28*, 2092−2100.

57. Collins, E. J., Garboczi, D. N., and Wiley, D. C. (1994) *Nature 371*, 626−629.

BI000749M